HYDROMAGNETIC NATURAL CONVECTION FROM AN INCLINED POROUS SQUARE ENCLOSURE WITH HEAT GENERATION

Khalil M. Khanafer and Ali J. Chamkha
Department of Mechanical and Industrial Engineering, College of Engineering and Petroleum, Kuwait University, P.O. Box 5969, Safat, Kuwait 13060

The problem of unsteady, laminar, two-dimensional hydromagnetic natural convection heat transfer in an inclined square enclosure filled with a fluid-saturated porous medium in the presence of a transverse magnetic field and fluid heat generation effects is studied numerically. The walls of the enclosure are maintained at constant temperatures. The flow in the porous region is modeled using the Brinkman–extended Darcy's law to account for the no-slip conditions at the walls. The control volume method is used to solve the governing balance equations for different values of the Darcy number, Hartmann number, and the inclination angle. Favorable comparisons with previously published work are performed. These comparisons confirmed the correctness of the numerical results. The obtained numerical results are presented graphically in terms of streamlines and isotherms as well as velocity and temperature profiles at midsections of the cavity to illustrate interesting features of the solution.

INTRODUCTION

Natural convection heat transfer in a porous medium induced by internal heat generation has recently received considerable attention because of numerous applications in geophysics and energy-related engineering problems [1–9]. Such applications include heat removal from nuclear fuel debris, underground disposal of radioactive waste materials, storage of foodstuff, and exothermic chemical reactions in packed-bed reactors [10]. Existing analyses on this phenomenon are based on the Darcy flow model due to its advantage in linearizing the momentum equation, which in turn removes a considerable amount of difficulty in solving the governing equations [11, 12]. However, the Darcy law cannot account for the no-slip boundary condition on the boundaries, which becomes important in porous media with high porosities such as foam metals and fibrous media [13]. Chan et al. [14] studied numerically natural convection heat transfer in enclosed porous media with rectangular boundaries using the Brinkman–extended Darcy model to satisfy both the impermeable and no-slip boundary conditions. Their results showed good agreement with experimental data. Emara and Kulacki [15] numerically analyzed thermal convection with a uniform volumetric energy source in a confined fluid with insulated side and bottom walls and rigid top wall or free top surface. It was

Received 8 October 1997; accepted 28 January 1998.
Address correspondence to Khalil M. Khanafer, College of Engineering and Petroleum, Department of Mechanical and Industrial Engineering, Kuwait University, P.O. Box 5969, Safat, Kuwait 13060.

Numerical Heat Transfer, Part A, 33:891–910, 1998

1040–7782/98 $12.00 + .00

NOMENCLATURE

a_{ij}	coefficient of finite difference equation at point (i, j) in a grid	V	dimensionless y component of velocity $(= v/\sqrt{g\beta\Delta TH})$
b	right-hand side of finite difference equation	V_c	dimensionless velocity in y direction at midwidth of enclosure
$\mathbf{B}$	magnetic induction vector, tesla	x, y	Cartesian coordinates
B_0	constant magnetic induction	X, Y	dimensionless Cartesian coordinates $[= (x, y)/H]$
c_p	fluid specific heat, J/(kg K)	α	enclosure inclination angle
Da	Darcy number $(= \kappa/H^2)$	α_e	effective thermal diffusivity of porous medium, m^2/s
Da^{-1}	inverse Darcy number $(= 1/Da)$	β	coefficient of thermal expansion of fluid, K^{-1}
g	gravitational acceleration, m/s^2	ΔT	temperature difference $(= q''' H^2/K_e)$
H	enclosure length, m	θ	dimensionless temperature $(= (T - T_c)/\Delta T]$
Ha	Hartmann number $(= B_0 H\sqrt{\sigma/\rho_0 \nu})$	κ	permeability of the porous medium, m^2
$\mathbf{J}$	current density vector, A/m^2	μ	effective dynamic viscosity, Pa s
K_e	effective thermal conductivity of the porous medium, W/(m, K)	ν	effective kinematic viscosity $(= \mu/\rho_0)$
L	characteristic length, m	ρ_0	fluid density at reference temperature T_c
M	grid number in x direction	σ	fluid electrical conductivity, mho
N	grid number in y direction	τ	dimensionless time $(= t\sqrt{g\beta\Delta TH}/H)$
$\overline{Nu}$	average Nusselt number, $[= -\int_0^1 (\partial\theta/\partial X)_{X=0}\, dY]$	ψ	stream function, $m^2 s$
P	fluid pressure, Pa	Ψ	dimensionless stream function $(= \psi/H\sqrt{g\beta\Delta TH})$
Pr	Prandtl number $(= \nu/\alpha_e)$	ω	dimensionless vorticity $(= \Omega H/\sqrt{g\beta\Delta TH})$
q'''	volumetric heat generation	Ω	dimensional vorticity, s^{-1}
Ra	Rayleigh number $(= g\beta q''' H^5/\nu\alpha_e K_e)$		
Ra_E	external Rayleigh number $(= g\beta\Delta TH^3/\nu\alpha_e)$, used in Table 3	**Subscripts**	
Ra_I	internal Rayleigh number $(= g\beta q''' H^5/\nu\alpha_e K_e)$, used in Table 3	c	cold wall
t	time, s	i	X location of a grid point
T	temperature, °C	j	Y location of a grid point
u	velocity in x direction		
U	dimensionless x component of velocity $(= u/\sqrt{g\beta\Delta TH})$		
v	velocity in y direction		
$\mathbf{V}$	velocity vector		

found from their results that the Nusselt numbers and the average temperature profiles within the fluid were in good agreement with experiment data. Later on, Beukema et al. [16] developed a three-dimensional model to study natural convection in a confined porous medium with internal heat generation. They applied this study to the storage process of agricultural products. Acharya and Goldstein [17] studied numerically two-dimensional natural convection of air in an externally heated vertical or inclined square box containing uniformly distributed internal

energy sources. Their numerical results showed two distinct flow pattern systems depending on the ratio of the internal to the external Rayleigh numbers. Also, it was found that the average heat flux ratio along the cold wall increased with increasing external Rayleigh number and decreasing internal Rayleigh number. Recently, Churbanov et al. [18] studied numerically unsteady natural convection of a heat-generating fluid in a vertical rectangular enclosure with isothermal or adiabatic rigid walls. Their results were obtained using a finite difference scheme in the two-dimensional stream function–vorticity formulation. Steady state as well as oscillating solutions were obtained and compared with other numerical and experimental published data. Other related works dealing with heat generation effects can be found in the papers by Vajravelu and Nayfeh [19] and Chamkha [20].

There has been considerable interest in studying the influence of a magnetic field on the performance of many systems using electrically conducting fluids. Some of these studies considered hydromagnetic flows and heat transfer in many different porous and nonporous geometries, e.g., [21–23]. This interaction was apparently first considered by Rapits et al. [24]. They studied the influence of the magnetic field on the free convection flow through a semi-infinite porous region bounded by two vertical infinite surfaces. Later, Rapits and Vlahos [25] investigated numerically the natural convection of a conducting fluid through a porous medium between two horizontal plates in the presence of a magnetic field. The effect of the transverse magnetic field on the natural convection of an electrically conducting fluid within an inclined porous tall enclosure with aspect ratio of 4 was investigated numerically as well as analytically by Vasseur et al. [26]. Their numerical results demonstrated that in the limit of high Ha, the resulting solution is equivalent to that obtained for a porous layer on the basis of Darcy's model. Recently, hydromagnetic natural convection of a conducting fluid through a porous medium has been studied by Bian et al. [27]. It is found that the temperature and the velocity fields are significantly modified with the application of the magnetic field.

The objective of the present work is to consider the Brinkman–extended Darcy equation of motion with the convective terms included and to examine the influence of the magnetic field and fluid heat generation effects on natural convection inside a tilted enclosure filled with a fluid-saturated porous medium for a wide range of inclination angles. Therefore, a two-dimensional numerical model will be used to solve the vorticity, stream function, and energy governing equations of buoyancy-driven natural convection flow inside the cavity.

PROBLEM FORMULATION

Consider unsteady, laminar, hydromagnetic natural convection flow in a two-dimensional inclined cavity of length H with isothermally cooled walls maintained at a constant temperature T_c as shown in Figure 1. The cavity is filled with a porous medium of uniform porosity and permeability saturated by an electrically conducting fluid that generates heat at a uniform rate. The fluid is permeated by a uniform externally applied magnetic field of strength B_0. No external electric field is assumed to exist, and the Hall effect of magnetohydrodynamics is negligible. The magnetic Reynolds number is assumed to be small so that the induced magnetic

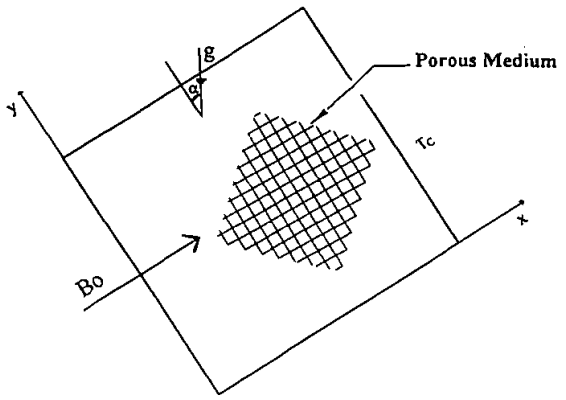

Figure 1. Schematic diagram of tilted porous-medium-filled square enclosure configuration with heat-generating fluid in the presence of a magnetic field effect.

field can be neglected compared to the applied magnetic field, as done by Garandet et al. [28]. The porous medium is assumed to be hydrodynamically, thermally, and electrically isotropic and saturated with a fluid that is in local thermodynamic equilibrium with solid matrix. The fluid is assumed to have constant physical properties except the density variation in the body force term of the momentum equation according to the Boussinesq approximation. In addition, pressure work, Joule heating, and viscous dissipation are all assumed negligible.

The pertinent governing equations for this study are based on the balance laws of mass, linear momentum, and energy modified to account for the presence of the buoyancy effect, porous medium, magnetic effect, and heat generation. These are given in vector form by

$$\nabla \cdot \mathbf{V} = 0 \tag{1}$$

$$\frac{\partial \mathbf{V}}{\partial t} + (\mathbf{V} \cdot \nabla)\mathbf{V} = -\frac{1}{\rho_0}\nabla P + \frac{\mathbf{J}}{\rho_0}\mathbf{x}\mathbf{B} + \nu\nabla^2\mathbf{V} - \beta(T - T_c)\mathbf{g} - \frac{\mu\mathbf{V}}{\rho_0 \kappa} \tag{2}$$

$$\rho_0 c_p \frac{DT}{Dt} = -\nabla \cdot q'' + \Phi + q''' + \frac{J^2}{\sigma} \tag{3}$$

$$\nabla \cdot \mathbf{J} = 0 \qquad \mathbf{J} = \sigma(-\nabla\varphi + \mathbf{V} \times \mathbf{B}) \tag{4}$$

where t stands for time; ∇ is the gradient operator; ∇^2 is the Laplacian operator; $\mathbf{g}$, $\mathbf{B}$, P, T, and $\mathbf{V}$ represent the gravitational acceleration vector, magnetic induction vector, pressure, temperature, and velocity vector, respectively; $\mathbf{J}$ is the current density vector; $-\nabla\varphi$ is the associated electric field; σ is the fluid electrical conductivity; β is the volumetric expansion coefficient; κ is the permeability of the porous medium; and ν, μ, ρ_0, and c_p are the effective kinematic viscosity, effective

dynamic viscosity, density, and specific heat, respectively. The terms J^2/σ, q''', and Φ in Eq. (3) are the dissipative Joule heating energy of the conducting fluid, the volumetric heat generation, and the viscous dissipation, respectively. In addition, $\frac{DT}{Dt}$ represents a substantial derivative.

Taking into account the preceding assumptions and defining the dimensionless stream function Ψ and the vorticity ω in the usual way, the dimensionless governing equations are transformed into

$$\omega = -\left(\frac{\partial^2\Psi}{\partial X^2} + \frac{\partial^2\Psi}{\partial Y^2}\right) \tag{5}$$

$$U = \frac{\partial\Psi}{\partial Y} \qquad V = -\frac{\partial\Psi}{\partial X} \tag{6}$$

$$\frac{\partial\omega}{\partial\tau} + U\frac{\partial\omega}{\partial X} + V\frac{\partial\omega}{\partial Y} = \sqrt{\frac{\mathrm{Pr}}{\mathrm{Ra}}}\left(\frac{\partial^2\omega}{\partial X^2} + \frac{\partial^2\omega}{\partial Y^2}\right) + \left(\frac{\partial\theta}{\partial X}\cos\alpha - \frac{\partial\theta}{\partial Y}\sin\alpha\right) - \sqrt{\frac{\mathrm{Pr}}{\mathrm{Ra}}}\,\mathrm{Ha}^2\frac{\partial V}{\partial X} - \sqrt{\frac{\mathrm{Pr}}{\mathrm{Ra}}}\,\frac{\omega}{\mathrm{Da}} \tag{7}$$

$$\frac{\partial\theta}{\partial\tau} + U\frac{\partial\theta}{\partial X} + V\frac{\partial\theta}{\partial Y} = \frac{1}{\sqrt{\mathrm{Ra}\,\mathrm{Pr}}}\left(\frac{\partial^2\theta}{\partial X^2} + \frac{\partial^2\theta}{\partial Y^2}\right) + \frac{1}{\sqrt{\mathrm{Ra}\,\mathrm{Pr}}} \tag{8}$$

The above equations have been reduced to dimensionless forms by using the following dimensionless variables:

$$X = \frac{x}{H} \qquad Y = \frac{y}{H}$$

$$U = \frac{u}{\sqrt{g\beta\Delta TH}} \qquad V = \frac{v}{\sqrt{g\beta\Delta TH}}$$

$$\theta = \frac{T - T_c}{\Delta T} \qquad \tau = \frac{t\sqrt{g\beta\Delta TH}}{H} \tag{9}$$

$$\omega = \frac{\Omega H}{\sqrt{g\beta\Delta TH}} \qquad \Psi = \frac{\psi}{H\sqrt{g\beta\Delta TH}}$$

$$\Delta T = \frac{q''' H^2}{K_e}$$

where Ω is the dimensional vorticity and K_e is the effective thermal conductivity of the porous medium.

The general transport equations of the vorticity or energy can be written in a canonical form as [29]

$$\frac{\partial \phi}{\partial \tau} + \frac{\partial}{\partial X}\left(U\phi - \Gamma_\phi \frac{\partial \phi}{\partial X}\right) + \frac{\partial}{\partial Y}\left(V\phi - \Gamma_\phi \frac{\partial \phi}{\partial Y}\right) = S_\phi \tag{10}$$

where ϕ stands for ω or θ and Γ_ϕ and S_ϕ are given by

$$\Gamma_\theta = \frac{1}{\sqrt{\mathrm{Ra}\,\mathrm{Pr}}} \qquad S_\theta = \frac{1}{\sqrt{\mathrm{Ra}\,\mathrm{Pr}}}$$

$$\Gamma_\omega = \sqrt{\frac{\mathrm{Pr}}{\mathrm{Ra}}} \qquad S_\omega = \left(\frac{\partial \theta}{\partial X}\cos\alpha - \frac{\partial \theta}{\partial Y}\sin\alpha\right) - \sqrt{\frac{\mathrm{Pr}}{\mathrm{Ra}}}\,\mathrm{Ha}^2 \frac{\partial V}{\partial X} - \sqrt{\frac{\mathrm{Pr}}{\mathrm{Ra}}}\,\frac{\omega}{\mathrm{Da}} \tag{11}$$

The physical initial and boundary conditions of the problem under consideration can be written in dimensionless form as

$$\begin{aligned} &U = V = \Psi = \theta = 0 \qquad \tau = 0 \\ &U = V = \Psi = \theta = 0 \qquad \tau > 0 \qquad \text{on all boundaries} \end{aligned} \tag{12}$$

An important physical characteristic for this heat transfer situation is the average Nusselt number at the left cold surface. This represents the average dimensionless heat transfer rate across the left cold surface and can be defined as

$$\overline{\mathrm{Nu}} = -\int_0^1 \left(\frac{\partial \theta}{\partial X}\right)_{X=0} dY \tag{13}$$

Similar expressions can be defined for the other sides of the cavity. For brevity, attention is focused on the average Nusselt number at the left cold surface only.

NUMERICAL ALGORITHM

In the present work the control volume algorithm [29] is used to solve the two-dimensional transient governing equations, Eq. (5)–(8), subject to the boundary conditions given in Eqs. (12). In this algorithm, the alternating direct implicit (ADI) procedure along with the successive grid refinement scheme are implemented in the spatial and temporal environment, respectively to accelerate the convergence of the solution toward steady state. Additionally, the application of the ADI procedure enhances the accuracy of the solution, sine it allows the power law scheme to be applied locally in a one-dimensional sense for each sweep in the coordinate directions. The resulting finite difference of Eq. (10) in the X and Y directions is given as

$$\begin{aligned} -a_{i-1,j}^{n+1/2}\phi_{i-1,j}^{n+1/2} + a_{i,j}^{n+1/2}\phi_{i,j}^{n+1/2} - a_{i+1,j}^{n+1/2}\phi_{i+1,j}^{n+1/2} &= b^n \\ -a_{i,j-1}^{n+1}\phi_{i,j-1}^{n+1} + a_{i,j}^{n+1}\phi_{i,j}^{n+1} - a_{i,j+1}^{n+1}\phi_{i,j+1}^{n+1} &= b^{n+1/2} \end{aligned} \tag{14}$$

where the subscripts i and j denote the X and Y locations of the grid point, respectively. The superscripts n, $n + 1/2$, and $n + 1$ denote old time, advanced half-time step, and advanced full-time step, respectively. The coefficients of Eqs. (14) are given by Patankar [29].

To complete the discretization process, the flow kinematics equation, Eq. (5), is discretized using central finite difference. The final form of the equations becomes

$$\Psi_{i,j}^{n+1} = \left(\Psi_{i,j}^{n+1}\right)^k + \frac{\lambda}{2(1+\varepsilon^2)} \times \left[\begin{array}{c} \left(\Psi_{i+1,j}^{n+1}\right)^k + \left(\Psi_{i-1,j}^{n+1}\right)^{k+1} + \varepsilon^2\left\{\left(\Psi_{i,j+1}^{n+1}\right)^k + \left(\Psi_{i,j-1}^{n+1}\right)^{k+1}\right\} \\ -2(1+\varepsilon^2)\left(\Psi_{i,j}^{n+1}\right)^k + \Delta X^2 \omega_{i,j}^{n+1} \end{array}\right] \tag{15}$$

where ε is the ratio of the step sizes, such that $\varepsilon = \Delta X/\Delta Y$, n and k are the time step and the iteration step, respectively, and λ represents the relaxation factor, which is given by

$$\lambda = \frac{8 - 4\sqrt{4 - \delta^2}}{\delta^2} \qquad \delta = \cos\left(\frac{\pi}{M}\right) + \cos\left(\frac{\pi}{N}\right) \tag{16}$$

where M and N are the total number of grid points along the X and Y directions, respectively. Once $\Psi_{i,j}^{n+1}$ is calculated, $U_{i,j}^{n+1}$ and $V_{i,j}^{n+1}$ are then computed from

$$\begin{aligned} U_{i,j}^{n+1} &= \frac{\Psi_{i,j+1}^{n+1} - \Psi_{i,j-1}^{n+1}}{2\Delta Y} \\ V_{i,j}^{n+1} &= \frac{\Psi_{i-1,j}^{n+1} - \Psi_{i+1,j}^{n+1}}{2\Delta X} \end{aligned} \tag{17}$$

The vorticity on the boundaries is computed according to the following expressions, which are obtained from Eqs. (5) and (6):

$$\begin{aligned} \omega_{i,1} &= \frac{(-4U_{i,2} + U_{i,3})}{2\Delta Y} \\ \omega_{i,N} &= \frac{(4U_{i,N-1} - U_{i,N-2})}{2\Delta Y} \\ \omega_{1,j} &= \frac{(4V_{2,j} - V_{3,j})}{2\Delta X} \\ \omega_{M,j} &= \frac{(-4V_{M-1,j} + V_{M-2,j})}{2\Delta X} \end{aligned} \tag{18}$$

SOLUTION PROCEDURE

1. Use the temperatures of the previous time step as an initial guess. For the first time step, the initial temperature will be used to initiate the computation.
2. Choose the trial values for U^n and V^n as the first approximations of U^{n+1} and V^{n+1}.
3. Compute the new values of the temperature at each grid point using Eq. (14) with ϕ playing the role of θ.
4. Use the values of the vorticities of the previous time step as an initial guess. For the first time step the vorticities are assumed to be zero everywhere to initiate the solution.
5. Use the values of U^{n+1}, V^{n+1}, and θ^{n+1} to compute the values of ω^{n+1} from Eq. (14) at the interior grid points.
6. Solve the stream function equation, Eq. (15), using the new values of the vorticities obtained in step 5.
7. Determine the new values of U^{n+1} and V^{n+1} from the values of ψ^{n+1} using the central difference formulae given by Eqs. (17).
8. Compute the new boundary vorticities using the new values of U^{n+1} and V^{n+1} obtained in step 7 using Eqs. (18).
9. Use the new values of U^{n+1} and V^{n+1} to repeat steps 5–8. Check the solution convergence of ω^{n+1} and θ^{n+1}, and if not converged, repeat steps 5–8.
10. Repeat steps 4–9 for advancing time levels until steady state convergence is achieved.

Numerical experiments performed to assess grid independence showed that an equally spaced grid mesh of 41 × 41 is adequate to describe correctly the flow and heat transfer processes. Further increase in the number of grid points produced essentially the same results. The convergence criterion employed to reach the steady state solution was the standard relative error, which is based on the maximum norm given by

$$\Delta = \frac{\|\Omega^{n+1} - \Omega^n\|_\infty}{\|\Omega^{n+1}\|_\infty} + \frac{\|\theta^{n+1} - \theta^n\|_\infty}{\|\theta^{n+1}\|_\infty} \leqslant 10^{-6} \tag{19}$$

where the operator $\|\eta\|_\infty$ indicates the maximum absolute value of the variable over all the grid points in the computational domain.

VALIDATION TESTS

The present numerical algorithm validated against the finite difference solution of Churbanov et al. [18] for a vertical square cavity with heat generation and in the absence of the magnetic field (Ha = 0) and the porous medium for Ra = 6.4 ×

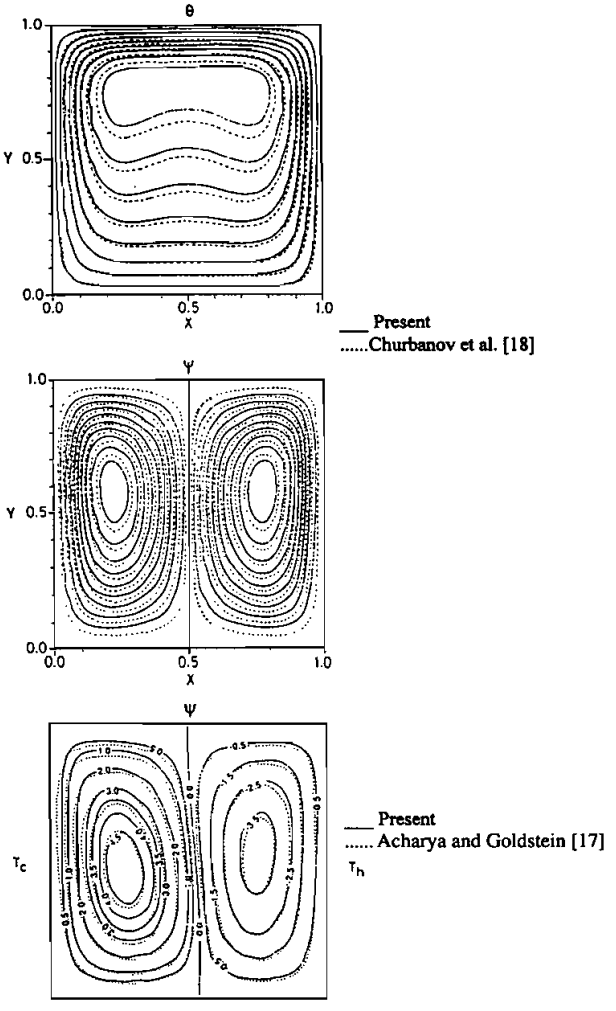

Figure 2. Comparison of steady state flow patterns and isothermal field of a vertical enclosure between the present prediction and other numerical results.

10^5 and Pr = 7.0 as shown in Figure 2. It can be seen from this figure that the two sets of contours are in good agreement. The slight discrepancies in these results are probably due to the use of different numerical techniques. Table 1 confirms the agreement of the values of Ψ_{max}, Ψ_{min}, θ_{max} and their locations for the present results and those reported by Churbanov et al. [18]. Moreover, Table 2 clearly shows and excellent agreement of the average heat flux ratio between the present solution and that of Acharya and Goldstein [17] inside a square tilted enclosure with heat generation. In addition to Table 2, the streamlines reported by Acharya and Goldstein [17] for internal and external Rayleigh numbers of 10^5 and 10^3, respectively, are reproduced and successfully compared as also shown in Figure 2.

Table 1. Comparison of the values of the stream function and their locations between the present solution and that of Churbanov et al. [18] for a vertical cavity with heat generation

Parameter	Present	Churbanov et al. [18]
$\Psi_{min}[X,Y]$	−0.8805 [0.775, 0.575]	−0.878 [0.775, 0.575]
$\Psi_{max}[X,Y]$	0.8805 [0.225, 0.575]	0.878 [0.225, 0.575]
$\theta_{max}[X,Y]$	0.04753 [0.3, 0.775]	0.0477 [0.3, 0.775]
	0.04753 [0.7, 0.775]	0.0477 [0.7, 0.775]

This comparison further confirms that the present numerical results are accurate. As an additional check on the accuracy of the results, the convergence of the numerical solution is checked by performing an overall heat transfer balance inside the cavity.

RESULTS AND DISCUSSION

In this section the numerical results are discussed in order to study the effects of the presence of the magnetic field, porous medium, and inclination angle of the natural convection of an electrically conducting and heat-generating fluid in a square cavity. Computations are carried out for $Ra = 6.4 \times 10^5$, as done by Churbanov et al. [18], Ha is ranging from 0 to 150, Da is ranging from 0 to 10^{-4}, and inclination angle $0° \leqslant \alpha \leqslant 90°$. The Prandtl number is fixed in all calculations at $Pr = 7$. Figure 3 shows typical streamlines and isotherms for a vertical cavity ($\alpha = 0°$) for $Ra = 6.4 \times 10^5$ and various values of the Ha in the absence of the porous medium. The influence of the magnetic field on the flow and temperature patterns is apparent from this figure. In the absence of the magnetic field, the flow and temperature patterns are similar to the results obtained by Churbanov et al. [18]. That is, the flow field circulates in the square cavity as two symmetrical counterrotating rolls moving upward close to the center of the cavity and downward near the two vertical cold walls. With the increase of the magnetic field, the flow circulation is progressively inhibited by the retarding effect of the hydromagnetic force such that the maximum intensity of circulation is $\Psi_{max} = 2.91 \times 10^{-3}$ for Ha = 0 but is only $\Psi_{max} = 4.99 \times 10^{-4}$ for Ha = 50. Furthermore, the circulation due to the convection effects within the cavity is inhibited. Thus the overall strength of the circulation is considerably reduced. For a high magnetic field,

Table 2. Comparison of the average heat flux ratio between the present solution and that of Acharya and Goldstein [17] for an inclination angle of 90° and $Ra_E = 10^3$ and $Ra_I = 10^5$

Parameter	Present	Acharya and Goldstein [17]
$\bar{q}_{r,c}$	0.989	0.99
$\bar{q}_{r,h}$	0.918	0.92

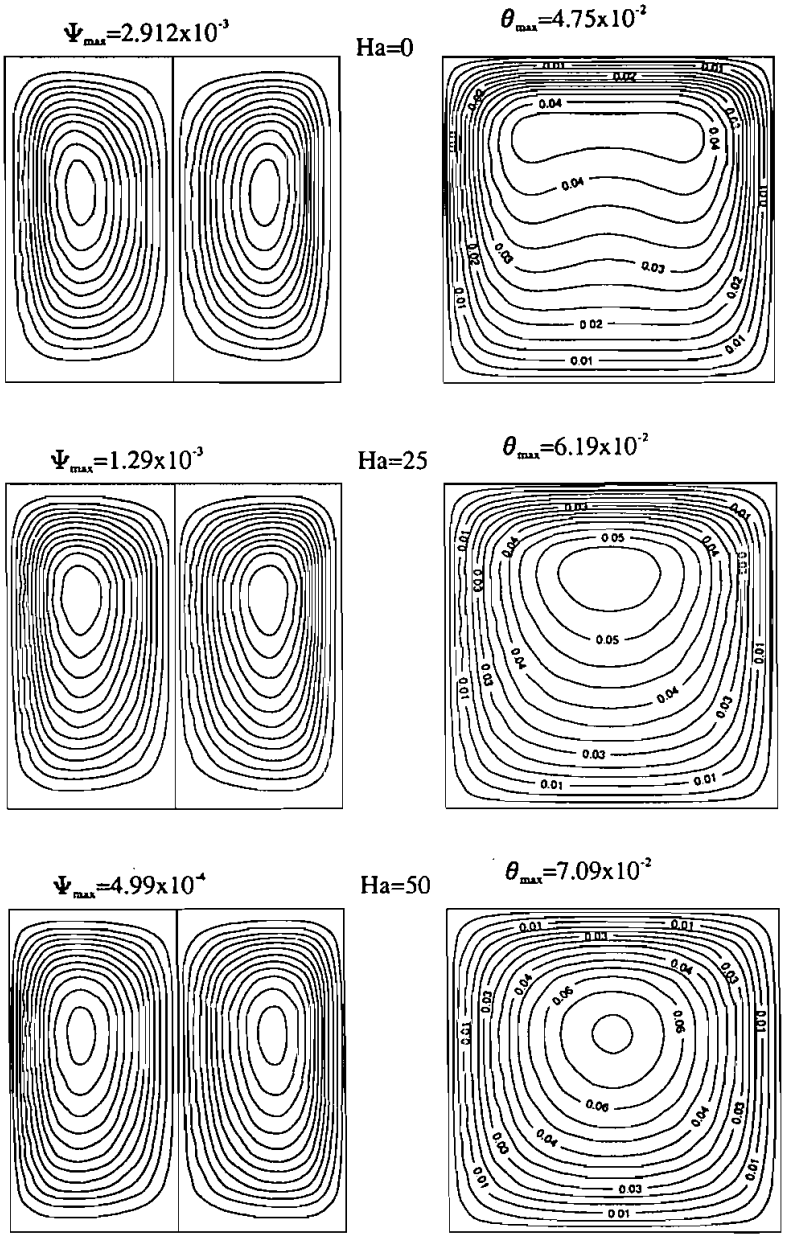

Figure 3. Steady state flow patterns and isothermal field of a vertical enclosure for various Hartmann numbers at Ra = 6.4×10^5 and Da = ∞.

Figure 3 shows that the convective motion inside the cavity is almost completely damped. Moreover, the isotherms at Ha = 50 comprise a unicellular heat flow, indicating that most of the heat transfer process is carried out by conduction. From the above, one can conclude that the main contribution of the magnetic effect is the suppression of the overall heat transfer in the cavity.

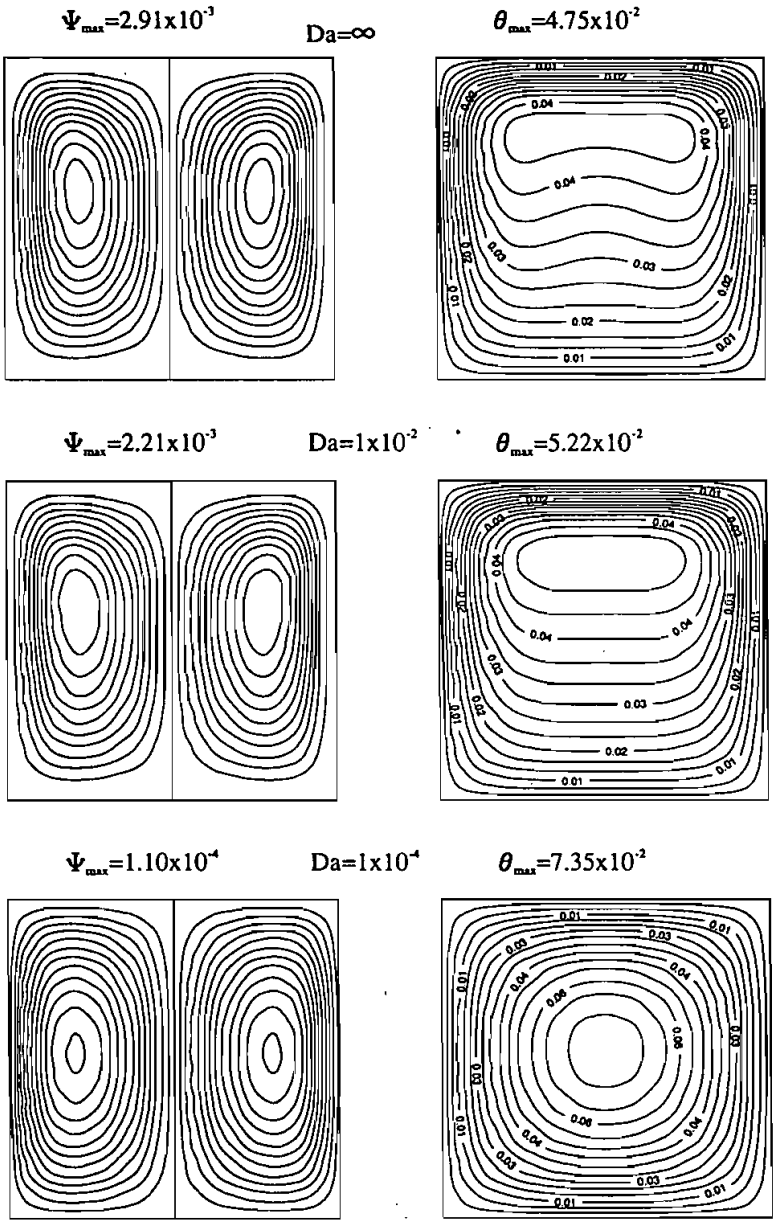

Figure 4. Steady state flow patterns and isothermal field of a vertical enclosure for various Darcy numbers at Ra = 6.4×10^5 and Ha = 0.

The effect of Da on the flow patterns and isotherms inside the cavity in the absence of the magnetic field at Ra = 6.4×10^5 is shown in Figure 4. It is clear from this figure that as Da decreases, the convective heat transfer decreases because of the retardation of the buoyancy force. A similar trend has been observed for strong magnetic field situations. As Da $\rightarrow \infty$, the flow patterns will be

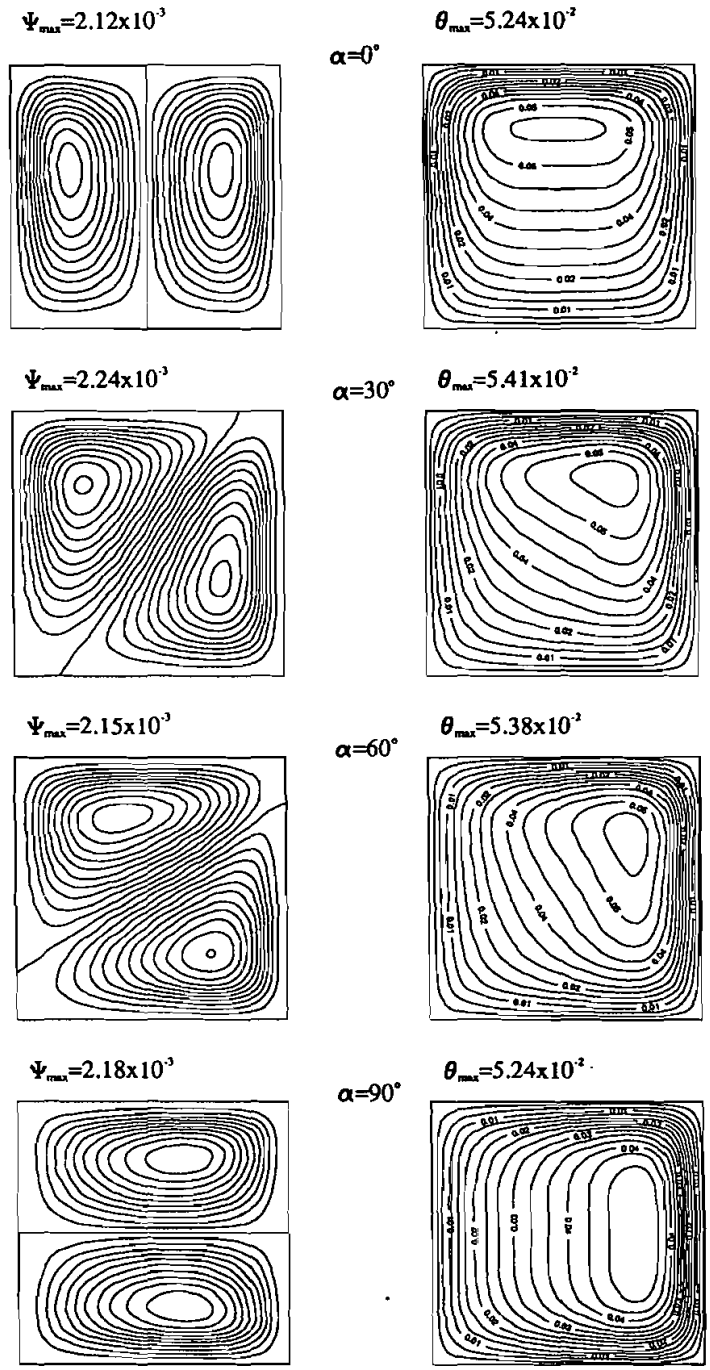

Figure 5. Steady state solution of flow patterns and isothermal field for various inclination angles at Ra = 6.4×10^5, Da = 1×10^{-2}, and Ha = 5.

that of the corresponding free convection problem with no porous medium. On the other hand, as Da decreases, the resistance to the flow caused by the presence of the porous medium increases. This causes the velocity of the fluid in the cavity to decrease. In the limit as Da $\rightarrow$ 0, the permeability of the medium approaches zero, causing the flow to eventually cease ($\Psi_{max} = 1.1 \times 10^{-4}$).

The influence of the inclination angle α on the flow patterns and isotherms in the presence of both the magnetic field and the porous medium is depicted in Figure 5. It is noticed from this figure that the maximum temperature occurs for an inclination angle of $\alpha = 30°$. Also, the comparison of the maximum value of the stream function at different inclination angles indicates that the flow field is fastest at 30° and slowest at 90°. The behavior is consistent with the earlier prediction reported by Acharya and Goldstein [17]. Moreover, it is evident from this figure

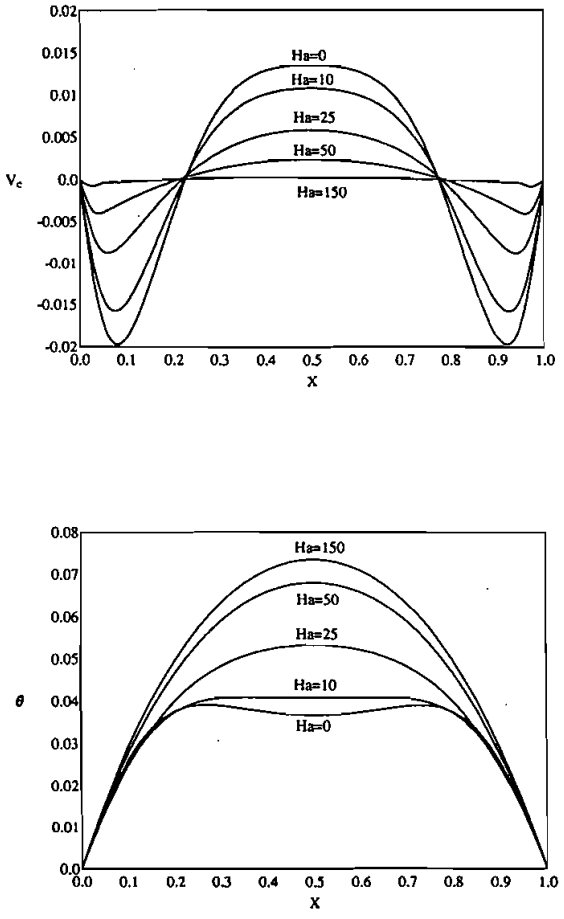

Figure 6. Vertical velocity and temperature profiles along the horizontal midheight of the vertical enclosure for various Hartmann numbers at Ra = 6.4×10^5 and Da = ∞.

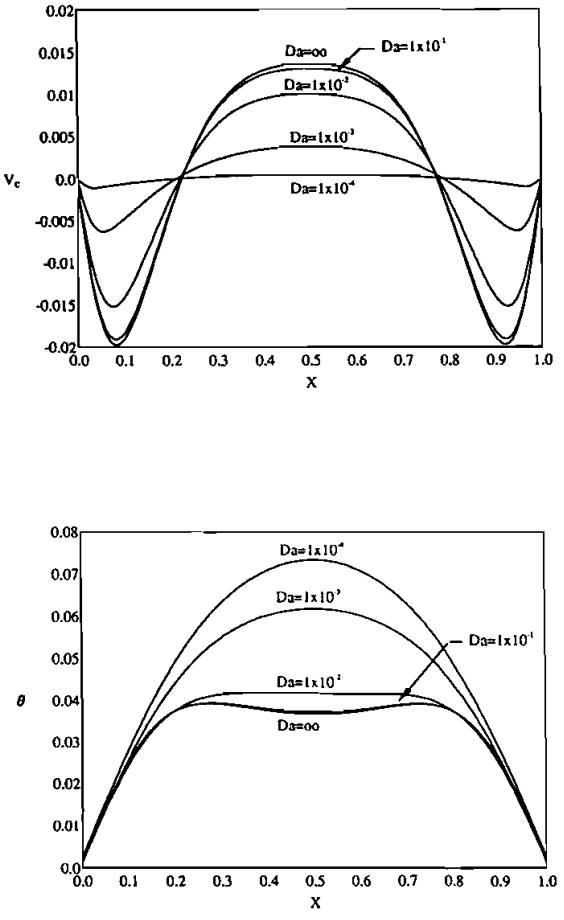

Figure 7. Vertical velocity and temperature profiles along the horizontal midheight of the vertical enclosure for various Darcy numbers at $Ra = 6.4 \times 10^5$ and $Ha = 0$.

that the axis between the two moving rolls rotates clockwise with the increase of the inclination angle until it finally becomes horizontal for $\alpha = 90°$. This is due to the effect of direction change of the buoyancy force. A similar behavior is also observed for the isotherms. As the inclination angle increases, the upper vortex as well as the isotherm lines rotate in the clockwise direction. At the end, the upper vortex elongates vertically, and vertical stratification is established for $\alpha = 90°$.

Typical temperature and velocity profiles in a vertical cavity ($\alpha = 0°$) for various values of the Ha, Da, and α at $Ra = 6.4 \times 10^5$ for midsections of the cavity are given in Figures 6–8. The application of a transverse magnetic field results in a force opposite to the flow direction, which tends to drag the flow. This

causes suppression in the thermal currents of the flow. Also the conduction heat transfer mechanism becomes dominant as either the Ha, the inverse Darcy number Da^{-1}, or the inclination angle increases. This is clearly noticed in the vertical velocity profiles at the center of the cavity depicted in Figures 6–8. It can be noticed that both the presence of the magnetic field and the porous medium play a similar role as flow resistance mechanisms.

Finally, the effects of Da, Ha, and α on $\overline{Nu}$ are shown in Figures 9*a*, 9*b*, and 9*c*, respectively. As discussed earlier, for a relatively high Ha or small Da the only resistance to the flow is due to the magnetic field and the porous medium, and the resulting convective heat transfer is diminished. Furthermore, it is observed from Figures 9*a* and 9*b* that for a specific value of Ha and Da^{-1}, $\overline{Nu}$ starts to increase

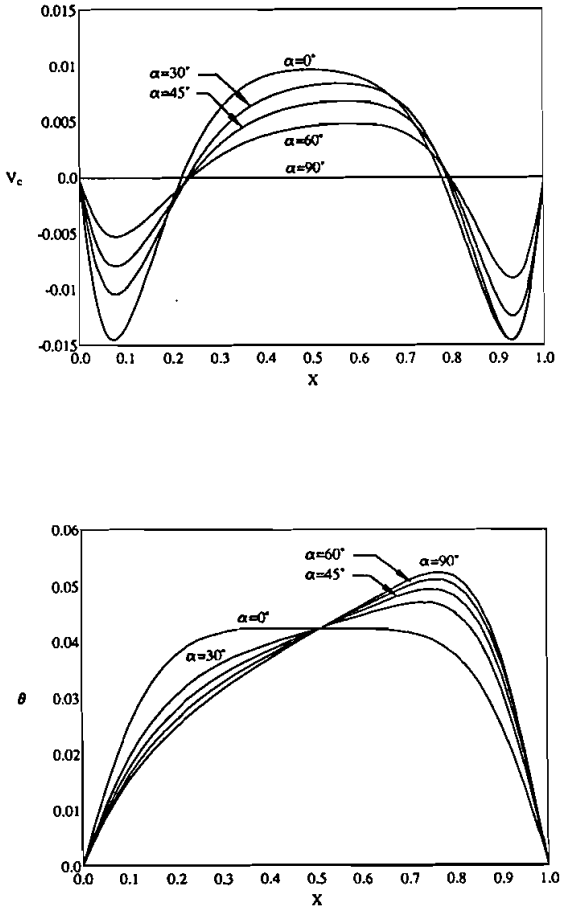

Figure 8. Vertical velocity and temperature profiles along the horizontal midheight of the enclosure for various inclination angles α at $Ra = 6.4 \times 10^5$, $Da = 1 \times 10^{-2}$, and $Ha = 5$.

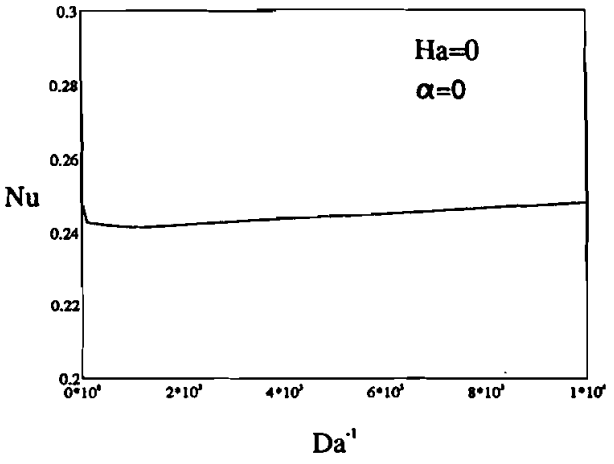

Figure 9*a*. Effect of Da^{-1} on the average Nusselt number.

and approaches a constant value, indicating a pure conduction regime. This means that the magnetic field and the porous medium have no effect on heat transfer in the case where the flow is totally ceased. In Figure 9*c* the rate of variation of $\overline{Nu}$ with the enclosure tilting angle is higher for small angles than for large angles.

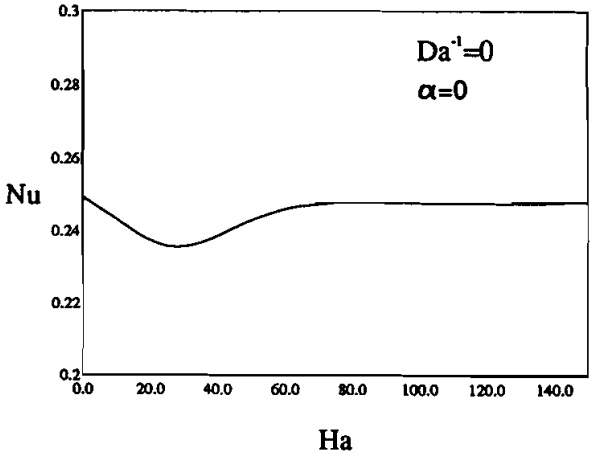

Figure 9*b*. Effect of Ha on the average Nusselt number.

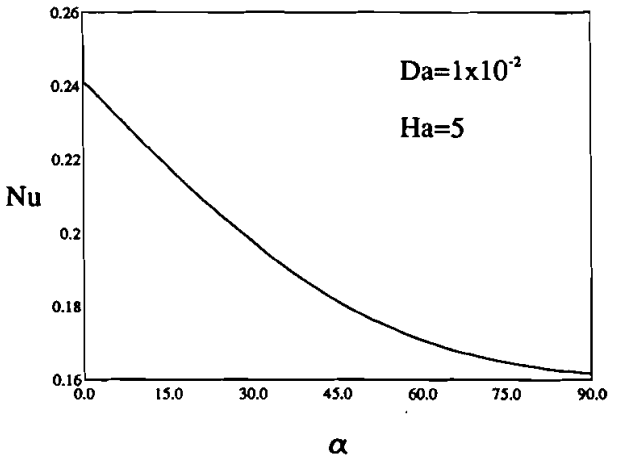

Figure 9c. Effect of α on the average Nusselt number.

CONCLUSIONS

Unsteady natural convection of a heat-generating fluid inside an inclined square porous cavity saturated with an electrically conducting fluid in the presence of a transverse magnetic field was studied numerically. The finite volume approach was employed along with alternating direction implicit scheme for the present problem. Comparisons with previously published work on special cases of the problem were performed and found to be in excellent agreement. Graphical results for various parametric conditions were presented and discussed. It was found that the heat transfer mechanisms and the flow characteristics inside the tilted enclosure depended strongly on the strength of the magnetic field, inclination angle, and Darcy number. Significant suppression of the convective currents was obtained by the application of a strong magnetic field and/or presence of a porous medium. Also, the effects of the magnetic field and the porous medium were found to reduce the heat transfer and fluid circulation within the cavity. In addition, it was concluded that the rate of variation of the average Nusselt number with the enclosure tilting angle is higher for small angles than for large angles.

REFERENCES

1. I. T. Hwang, Finite Amplitude Thermal Convection in Porous Media with Heat Source and Variable Viscosity, Ph.D. thesis, University of Minnesota, 1971.
2. F. A. Kulacki and R. Ramchandani, Hydrodynamic Instability in a Porous Layer Saturated with a Heat Generating Fluid, *Warme-Stoffubertragung*, vol. 8, pp. 179–185, 1975.
3. R. D. Gasser and M. S. Kazimi, Onset of Convection in a Porous Medium with Internal Heat Generation, *ASME J. Heat Transfer*, vol. 98, pp. 49–54, 1976.

4. R. J. Burreta and A. S. Berman, Convection Heat Transfer in a Liquid Saturated Porous Layer, *ASME J. Heat Transfer*, vol. 98, pp. 249–253, 1976.
5. H. C. Hardee and R. H. Nilson, Natural Convection in Porous Media with Heat Generation, *Nucl. Sci. Eng.*, vol. 63, pp. 119–132, 1977.
6. F. A. Kulacki and R. G. Freeman, A Note on Thermal Convection in a Saturated Heat Generating Porous Layer, *ASME J. Heat Transfer*, vol. 101, pp. 169–171, 1979.
7. L. Baker Jr., R. E. Faw, and E. A. Kulacki, Postaccidental Heat Removal—Part I: Heat Transfer Within Internally Heated Nonboiling Liquid Layer, *Nucl. Sci. Eng.* vol. 66, pp. 223–230, 1976a.
8. L. Baker Jr., R. E. Faw, and E. A. Kulacki, Postaccidental Heat Removal—Part II: Heat Transfer Within Internally Heated Liquid to a Melting Solid, *Nucl. Sci. Eng.*, vol. 66, pp. 231–238, 1979b.
9. S. K. Runcorn, Convection Current in the Earth's Mantle, *Nature*, vol. 95, pp. 1248–1249, 1962.
10. S. Kakac, W. Aung, and R. Viskanta, *Natural Convection—Fundamentals and Applications*, Hemisphere, Washington, D. C., 1985.
11. V. Prasad, Thermal Convection in a Rectangular Cavity Filled with a Heat-Generating, Darcy Porous Medium, *ASME J. Heat Transfer*, vol. 109, pp. 697–703, 1987.
12. M. Haajizadeh, A. F. Ozguc, and C. L. Tien, Natural Convection in a Vertical Porous Enclosure with Internal Heat Generation, *Int. J. Heat Mass Transfer*, vol. 27, no. 10, pp. 1893–1902, 1984.
13. P. Vasseur and L. Robillard, The Brinkman Model for Boundary Layer Regime in a Rectangular Cavity with Uniform Heat Flux from the Side, *Int. J. Heat Mass Transfer*, vol. 30, no. 4, pp. 717–727, 1987.
14. B. K. C. Chan, C. M. Ivey, and J. M Barry, Natural Convection in Enclosed Porous Media with Rectangular Boundaries, *ASME J. Heat Transfer*, vol. 92, pp. 21–27, 1970.
15. A. A. Emara and F. A. Kulacki, A Numerical Investigation of Thermal Convection in a Heat-Generating Fluid Layer, ASME Paper No. 79-HT-103.
16. K. J. Keukema, S. Bruin, and J. Schenk, Three-Dimensional Natural Convection in a Confined Porous Medium with Internal Heat Generation, *Int. J. Heat Mass Transfer*, vol. 26, pp. 451–458, 1983.
17. S. Acharya and R. J. Goldstein, Natural Convection in an Externally Heated Vertical or Inclined Square Box Containing Internal Energy Sources, *ASME J. Heat Transfer*, vol. 107, pp. 855–866, 1985.
18. A. G. Churbanov, P. N. Vabishchevich, V. V. Chudanov, and V. F. Strizhov, A Numerical Study on Natural Convection of a Heat-Generating Fluid in Rectangular Enclosures, *Int. J. Heat Mass Transfer*, vol. 37, no. 18, pp. 2969–2984, 1994.
19. K. Vajravelu and J. Nayfeh, Hydromagnetic Convection at a Cone and a Wedge, *Int. Commun. Heat Mass Transfer*, vol. 19, pp. 701–710, 1992.
20. A. J. Chamkha, Non-Darcy Fully Developed Mixed Convection in a Porous Medium Channel with Heat Generation/Absorption and Hydromagnetic Effects, *Numer. Heat Transfer*, vol. 32, pp. 653–675, 1997.
21. N. G. Kafoussias, MHD Free Convection Flow Through a Nonhomogeneous Porous Medium over an Isothermal Cone Surface, *Mech. Res. Commun.*, vol. 19, pp. 89–94, 1992.
22. T. K. Aldoss, M. A. Al-Nimr, M. A. Jarrah, and B. J. Al-Sha'er, Magnetohydrodynamic Mixed Convection from a Vertical Plate Embedded in a Porous Medium, *Numer. Heat Transfer*, part A, vol. 28, pp. 635–645, 1995.
23. A. J. Chamkha, Non-Darcy Hydromagnetic Free Convection from a Cone and a Wedge in Porous Medium, *Int. Commun. Heat Mass Transfer*, vol. 23, pp. 875–887, 1996.

24. A. Rapits, C. Masslas, and G. Tzivanidis, Hydromagnetic Free Convection Flow Through a Porous Medium Between Two Parallel Plates, *Phys. Lett.*, vol. 90A pp. 288–289, 1982a.
25. A. Rapits and J. Vlahos, Unsteady Hydromagnetic Free Convection Flow Through a Porous Medium, *Lett. Heat Mass Transfer*, vol. 9, pp. 56–64, 1982b.
26. P. Vasseur, M. Hasnaoui, E. Bilgen, and L. Robillard, Natural Convection in an Inclined Fluid Layer with a Transverse Magnetic Field: Analogy with a Porous Medium, *ASME J. Heat Transfer*, vol. 117, pp. 121–129, 1995.
27. W. Bian, P. Vasseur, E. Bilgen, and F. Meng, Effect of an Electromagnetic Field on Natural Convection in an Inclined Porous Medium, *Int. J. Heat Fluid Flow*, vol. 17, pp. 36–44, 1996.
28. J. P. Garandet, T. Alboussiere, and R. Moreau, Buoyance Driven Convection in a Rectangular Enclosure with a Transverse Magnetic Field, *Int. J. Heat Mass Transfer*, vol. 35, no. 4, pp. 741–748, 1992.
29. S. V. Patankar, *Numerical Heat Transfer and Fluid Flow*, Hemisphere, Washington, D.C., 1980.